Clinical Cancer Research

Tumor-Infiltrating Plasma Cells Are Associated with Tertiary Lymphoid Structures, Cytolytic T-Cell Responses, and Superior Prognosis in Ovarian Cancer

David R. Kroeger[1], Katy Milne[1], and Brad H. Nelson[1,2,3]

Abstract

Purpose: $CD8^+$ tumor-infiltrating lymphocytes (TIL) are key mediators of antitumor immunity and are strongly associated with survival in virtually all solid tumors. However, the prognostic effect of $CD8^+$ TIL is markedly higher in the presence of $CD20^+$ B cells, suggesting that cooperative interactions between these lymphocyte subsets lead to more potent antitumor immunity.

Experimental Design: We assessed the colocalization patterns, phenotypes, and gene expression profiles of tumor-associated T- and B-lineage cells in high-grade serous ovarian cancer (HGSC) by multicolor IHC, flow cytometry, and bioinformatic analysis of gene expression data from The Cancer Genome Atlas.

Results: T cells and B cells colocalized in four types of lymphoid aggregate, ranging from small, diffuse clusters to large, well-organized tertiary lymphoid structures (TLS) resembling activated lymph nodes. TLS were frequently surrounded by dense infiltrates of plasma cells (PC), which comprised up to 90% of tumor stroma. PCs expressed mature, oligoclonal IgG transcripts, indicative of antigen-specific responses. PCs were associated with the highest levels of $CD8^+$, $CD4^+$, and $CD20^+$ TIL, as well as numerous cytotoxicity-related gene products. $CD8^+$ TIL carried prognostic benefit only in the presence of PCs and these other TIL subsets. PCs were independent of mutation load, *BRCA1/2* status, and differentiation antigens but positively associated with cancer–testis antigens.

Conclusions: PCs are associated with the most robust, prognostically favorable $CD8^+$ TIL responses in HGSC. We propose that TLS facilitate coordinated antitumor responses involving the combined actions of cytolytic T cells and antibody-producing PCs. *Clin Cancer Res; 22(12); 3005–15. ©2016 AACR.*

Introduction

To mediate effective tumor control, the immune system must contend with the spatial heterogeneity and dynamic evolutionary processes that characterize human cancer. Advanced carcinomas are composed of multiple subclones that, despite a common cellular origin and shared founder mutations, show divergent genetic, biologic, clinical, and immunologic properties (1). Moreover, the subclonal structure of cancers continually evolves in response to the selective pressures imposed by the host and the cytotoxic effects of treatment (2). Tumor evolution can lead to the emergence of treatment-resistant variants that ultimately give rise to fatal disease. Yet at the same time, emerging tumor variants can express novel antigens that instigate new cycles of immune recognition and attack. Thus, for the immune system to successfully contend with advanced cancers, it must deploy surveillance and effector mechanisms that continually adapt to the evolving tumor. Understanding these mechanisms is essential for the development of immunotherapies that yield durable responses.

These concepts are well illustrated by high-grade serous ovarian cancer (HGSC; ref. 3). At the genomic level, HGSC is characterized by near universal mutations in the tumor suppressor *TP53*, as well as frequent disruption of *BRCA1*, *BRCA2*, or other genes involved in homologous DNA repair, resulting in a high degree of genomic instability (4). Although HGSC has an intermediate mutation load, tumors show extensive copy number variation (4). Compounding this genomic complexity, HGSC disseminates early and extensively and typically is not detected until advanced stages (3). As a result, HGSC exhibits a high degree of spatial heterogeneity involving potentially dozens of genomically distinct subclones with extensive dissemination across metastatic sites (5–7). Although HGSC is highly sensitive to primary platinum-based chemotherapy, the development of chemoresistant disease is common and can bring profound changes in subclonal architecture and mutation profiles (6–8).

Despite this complexity, there is a strong link between antitumor immunity and patient survival in HGSC, suggesting the immune system can contend with tumor heterogeneity in a substantial proportion of cases. In particular, the presence of $CD8^+$ tumor-infiltrating lymphocytes (TIL) in primary tumors carries a >2-fold increased likelihood of survival (9). Importantly, however, $CD8^+$ TILs do not operate in isolation. We have shown

[1]Deeley Research Centre, British Columbia Cancer Agency, Victoria, British Columbia, Canada. [2]Department of Biochemistry and Microbiology, University of Victoria, Victoria, British Columbia, Canada. [3]Department of Medical Genetics, University of British Columbia, Vancouver, British Columbia, Canada.

Note: Supplementary data for this article are available at Clinical Cancer Research Online (http://clincancerres.aacrjournals.org/).

Corresponding Author: Brad H. Nelson, British Columbia Cancer Agency, 2410 Lee Avenue, Victoria, BC V8R 6V5, Canada. Phone: 250-519-5705; Fax: 125-0519-2004; E-mail: bnelson@bccrc.ca

doi: 10.1158/1078-0432.CCR-15-2762

Translational Relevance

The role of B cells in anticancer immunity remains controversial. Our data directly address this controversy by demonstrating that plasma cells (PCs) are an integral component of $CD8^+$ tumor-infiltrating lymphocyte responses. We show that the well-established prognostic benefit of $CD8^+$ TIL is restricted to tumors that additionally harbor PCs. Our findings indicate that, rather than working in opposition, the B-cell and T-cell lineages mount closely integrated responses to human tumors as reflected by their physical colocalization, synergistic functional profiles, and interdependent prognostic significance. We discuss the implications of these findings for the development of immunotherapies that engage and fortify intrinsic tumor surveillance mechanisms to achieve more durable clinical responses.

that tumors containing $CD8^+$ TIL are often additionally infiltrated by $CD20^+$ B cells (10,11). $CD20^+$ TIL exhibit an antigen-experienced, IgG-positive memory phenotype (11). Importantly, tumors containing both $CD8^+$ and $CD20^+$ TIL are associated with higher survival rates than those containing $CD8^+$ TIL alone. Similar results have been reported in a variety of other cancers (12–14), suggesting that effective tumor immunity involves cooperative interactions between T cells and B cells.

In our prior study (11), we found that $CD8^+$ and $CD20^+$ TIL often colocalized in lymphoid aggregates of various sizes and morphology. This is reminiscent of autoimmune conditions, where lymphoid aggregates develop in affected tissues. In rheumatoid arthritis, lymphoid aggregates have been classified into three grades, ranging from small perivascular collections of B and T cells (grade I) to large, highly organized structures resembling lymph nodes (grade III; ref. 15). These latter aggregates, referred to as tertiary lymphoid structures (TLS), are found not only in autoimmunity, but also in chronic infection, graft rejection, and cancer (16). Like conventional lymph nodes, TLSs harbor prominent B-cell follicles adjoined by discrete T-cell zones containing $CD4^+$ and $CD8^+$ T cells, dendritic cells, and high endothelial venules (HEV; ref. 16). The B-cell follicles of active TLS contain germinal centers (GC) with interdigitating networks of follicular DCs (fDC). In the setting of cancer, TLS are receiving increased attention, as they have been associated with favorable prognosis in several solid tumors (17–19).

To better understand the mechanisms by which T cells and B cells work together to mediate antitumor immunity, we investigated the colocalization patterns, phenotypes, and gene expression profiles of tumor-associated T- and B-lineage cells in HGSC. We found that the most robust, prognostically favorable $CD8^+$ TIL responses are accompanied not only by $CD20^+$ TIL but by dense stromal infiltrates of IgG^+ plasma cells. We propose that optimal antitumor immunity may involve closely integrated cytolytic- and antibody-mediated effector mechanisms.

Materials and Methods

Additional information is provided in Supplementary Materials.

Patient cohorts

The study protocol was approved by the Research Ethics Board of the BC Cancer Agency and University of British Columbia (Vancouver, BC). HGSC tumor specimens were obtained from previously untreated patients from a prospective cohort (treated from 2007–present) or retrospective cohort (optimally debulked cases treated from 1984–2000; Supplementary Table S4; refs. 10,20). Bioinformatic analyses utilized data from 570 untreated HGSC cases from The Cancer Genome Atlas (TCGA; ref. 4).

IHC and image analysis

Antibodies are listed in Supplementary Table S6. Multicolor IHC of formalin-fixed paraffin-embedded (FFPE) tissue was performed using previously described methods (11). Slides were scanned with an Aperio ScanScope (Leica Biosystems) and analyzed using ImageScope software v12.1 (Aperio Technologies) with the Stereology Toolkit v4.2.0 (ADCIS). TILs were enumerated in ten random 20× fields, and cell counts were normalized to the area of tumor epithelium evaluated. PC density was measured using a 4-point scale (21); for survival analyses, cases with PC scores ≥ 1 were deemed positive.

Flow cytometry

Disaggregated tumor cell suspensions were washed and labeled with fluorophore-conjugated monoclonal antibodies (Supplementary Table S6). Flow cytometry and sorting were performed using a BD Influx instrument.

IgG sequence analysis

RNA was extracted from FACS-purified memory B cells and plasma cells ($1–5 \times 10^3$ each) and bulk tumor cells (2.5×10^6). PCR reactions were performed using primers designed to amplify all *IGHG* variable regions. Up to 192 clones per sample were subjected to Sanger sequencing.

NanoString gene expression analysis

Total RNA was prepared from FFPE whole tumor sections using the AllPrep DNA/RNA FFPE Kit (Ambion, Life Technologies). Total RNA (200 ng) was analyzed using the PanCancer Immune Profiling Panel and nCounter platform (NanoString Technologies). Data were normalized using nSolver Software.

Bioinformatic analysis

The HGSC gene expression array dataset from TCGA was downloaded from bioconductor.org. Corresponding RNA-seq data, nonsynonymous point mutation counts, *BRCA1*, *BRCA2*, and *TP53* mutation status, and *BRCA1* promoter methylation calls were appended.

Statistical analysis

Statistical analyses were performed using R v3.1.1 and GraphPad Prism v6.0.

Results

Multicolor IHC reveals four types of lymphoid aggregates in HGSC

To visualize the different lymphoid aggregates present in HGSC, we developed a 6-color IHC panel that enabled simultaneous detection of $CD8^+$ and $CD4^+$ ($CD3^+CD8^-$) T cells, $CD20^+$

B cells, $CD21^+$ fDC, $CD208^+$ activated conventional DC, and $PNAd^+$ HEV-like vessels. The panel was applied to whole sections from 30 randomly selected HGSC tumors. To control for anatomic location, we stained an equal number of specimens from ovary or omentum; for 7 cases, we stained matched ovary and omentum samples to allow direct comparison between these sites.

We observed a variety of lymphoid aggregates, which we classified into four types based on size, cellular composition, and degree of organization. Type I aggregates were small (approximately 20–50 cells), compact, and composed of $CD4^+$ and $CD8^+$ T cells, B cells, and occasional DCs (Fig. 1A), thereby resembling grade I aggregates in rheumatoid arthritis (15). Type II aggregates were larger (100–>1000 cells) and composed of $CD4^+$ and $CD8^+$ T cells and $CD20^+$ B cells (Fig. 1B). These aggregates were diffuse and lacked discrete zones or follicles. Type III aggregates represented fully developed TLS, similar to grade III aggregates in rheumatoid arthritis (15). TLS had prominent B-cell follicles with GC-like structures characterized by interdigitating networks of $CD21^+$ fDC. In addition, they contained discrete T-cell zones with $CD4^+$ and $CD8^+$ T cells, DCs, and $PNAd^+$ HEV-like vessels (Fig. 1C). Finally, type IV aggregates were composed of approximately 100 to 300 $CD20^+$ B cells and fDC organized into follicles with few $CD4^+$ and $CD8^+$ T cells (Fig. 1D). As these structures did not contain clear T-cell zones and were primarily (6/7) found in omental samples, we speculated many or all were normal milky spots (22).

The four types of aggregates were strongly associated with one another. Type I and II aggregates were found in the same 17 of 30 tumors. TLS were found in 7 of 30 tumors, all of which contained type I and II aggregates. Type IV aggregates were observed in 7 of 30 tumors, of which 7 of 7 contained type I and II aggregates and 5 of 7 contained TLS. There was a trend toward a higher prevalence of type I–III aggregates in omental versus ovarian samples; however, this did not reach statistical significance. Given their high degree of coincidence, type I–III aggregates could represent a developmental continuum of structures, as has been suggested for similar aggregates in rheumatoid arthritis (15). Alternatively, they could reflect distinct immunologic processes underway in the tumor microenvironment.

All four types of aggregates were strongly associated with TIL. Tumors containing type I or II aggregates were positive for $CD4^+$ and $CD8^+$ TIL in 17 of 17 cases and $CD20^+$ TIL in 14 of 17 cases. Likewise, all tumors containing TLS (7/7) contained $CD4^+$, $CD8^+$, and $CD20^+$ TIL (Fig. 1E). We compared the density of TIL in TLS-proximal (<500 μm from the TLS center) versus TLS-distal (>500 μm) tumor regions. $CD20^+$ TIL showed a >10-fold greater density in TLS-proximal epithelium (28.5 vs. 2.5 cells/20× field; $P = 0.013$, Mann–Whitney test; Fig. 1F). $CD4^+$ and $CD8^+$ TIL showed a similar trend (72 vs. 24 and 227 vs. 59 cells/20× field, respectively), although this did not reach statistical significance (Fig. 1F). TIL densities were similar between omental and ovarian sites (all $P > 0.4$, Mann–Whitney test).

TLS are associated with dense plasma cell infiltrates in tumor stroma

To investigate whether the GC-like structures observed in TLS were sites of B-cell differentiation, sections containing TLS were subjected to 3-color IHC with antibodies to BCL-6, CD3, and CD20. We detected nuclear expression of BCL-6 in both $CD20^+$ and $CD3^+$ cells within B-cell follicles, indicating the presence of GC B cells and follicular helper T cells (Tfh), respectively (Fig. 2A). Moreover, virtually all TLS contained AID^+ $CD20^+$ B cells, which are indicative of ongoing immunoglobulin class switching and somatic hypermutation (Fig. 2B). BCL-6^+ and AID^+ B cells were also observed in type IV aggregates, but not type I or II aggregates. Thus, TLS exhibited the hallmarks of ongoing GC reactions.

Tumors were stained with antibodies to CD38, CD138, and CD79a to distinguish PCs (which are $CD20^-$ but coexpress CD38, CD138, and cytosolic CD79a) from naïve and memory B cells (which are $CD38^-CD138^-$ but express membranous CD79a) and $CD138^+$ tumor or stromal cells. PCs were found in 21 of 30 tumors and generally formed dense stromal infiltrates, constituting 50% to 90% of stromal cells (Fig. 2C and D). PCs were typically concentrated near the periphery of TLS (Fig. 2E). In several cases, $CD138^+$ cells were observed in GCs (Fig. 2F). There was a strong association between TLS and the density of stromal PCs (mean PC score in the presence of TLS = 2.6 vs. 1.0 in the absence of TLS, $P = 0.0004$, Mann–Whitney test; Fig. 2G), although 2 of 30 tumors contained abundant PCs (PC score of 3) in the absence of TLS (Fig. 2G). Thus, TLS-associated GCs could serve as sites of PC differentiation. The density of PCs was also positively associated with the intraepithelial density of $CD4^+$, $CD8^+$, and $CD20^+$ TIL (all Spearman $r > 0.6$, $P < 0.001$; Fig. 2F).

A coordinated antitumor response including PCs is associated with survival in HGSC

To assess the prognostic significance of tumor-associated PCs, we analyzed a retrospective HGSC tissue microarray, which has been previously evaluated for numerous TIL subsets (10,11,23). Consistent with our initial immunohistochemical analysis, PCs were found in 36% (62/172) of cases and showed a predominantly stromal location. When PCs were considered in relation to other TIL subsets, 90% of cases (155/172) fell into one of six subgroups: (i) no TIL (11% of cases); (ii) $CD8^+$ TIL alone (7.5%); (iii) $CD8^+$ and $CD4^+$ TIL (20%); (iv) $CD8^+$ and $CD4^+$ TIL with PCs (13%); (v) $CD8^+$, $CD4^+$, and $CD20^+$ TIL (16%); and (vi) $CD8^+$, $CD4^+$, and $CD20^+$ TIL with PCs (23%; Fig. 3A). These subgroups were associated with stepwise increases in the densities of $CD8^+$, $CD4^+$, and $CD20^+$ TIL (all ANOVA $P < 0.0001$). The density of $CD25^+FoxP3^+$ TIL (23) followed a similar pattern (ANOVA $P = 0.0007$). TIL patterns showed no association with patient age or stage of disease (ANOVA $P = 0.777$, $\chi^2 P = 0.6173$, respectively). Thus, PCs were associated with increasingly dense infiltrates of both effector and regulatory T cells.

The six subgroups carried distinct prognostic significance (Fig. 3B). The survival rate associated with $CD8^+$ TIL alone was similar to tumors lacking TIL altogether. Of tumors containing $CD8^+$ TIL, those that additionally contained $CD4^+$ TIL, CD20+ TIL, or PCs were associated with minor, statistically insignificant increases in survival. However, tumors containing $CD8^+$, $CD4^+$, and $CD20^+$ TIL together with PCs were associated with markedly increased survival, with approximately 65% of patients alive at 10 years. Thus, the prognostic benefit of $CD8^+$ TIL was restricted to tumors that additionally harbor PCs and these other TIL subsets.

Tumor-associated PCs are IgG^+CXCR3^+ and clonally expanded

The phenotype of PCs was further defined by flow cytometry of disaggregated viable tumor samples corresponding to 12 of 30 cases used in our multicolor IHC analysis above (Figs. 1 and 2). The proportion of $CD19^+$ B cells varied widely between tumors (mean = 6.1% of viable lymphocytes; range = 0.4–30). On the

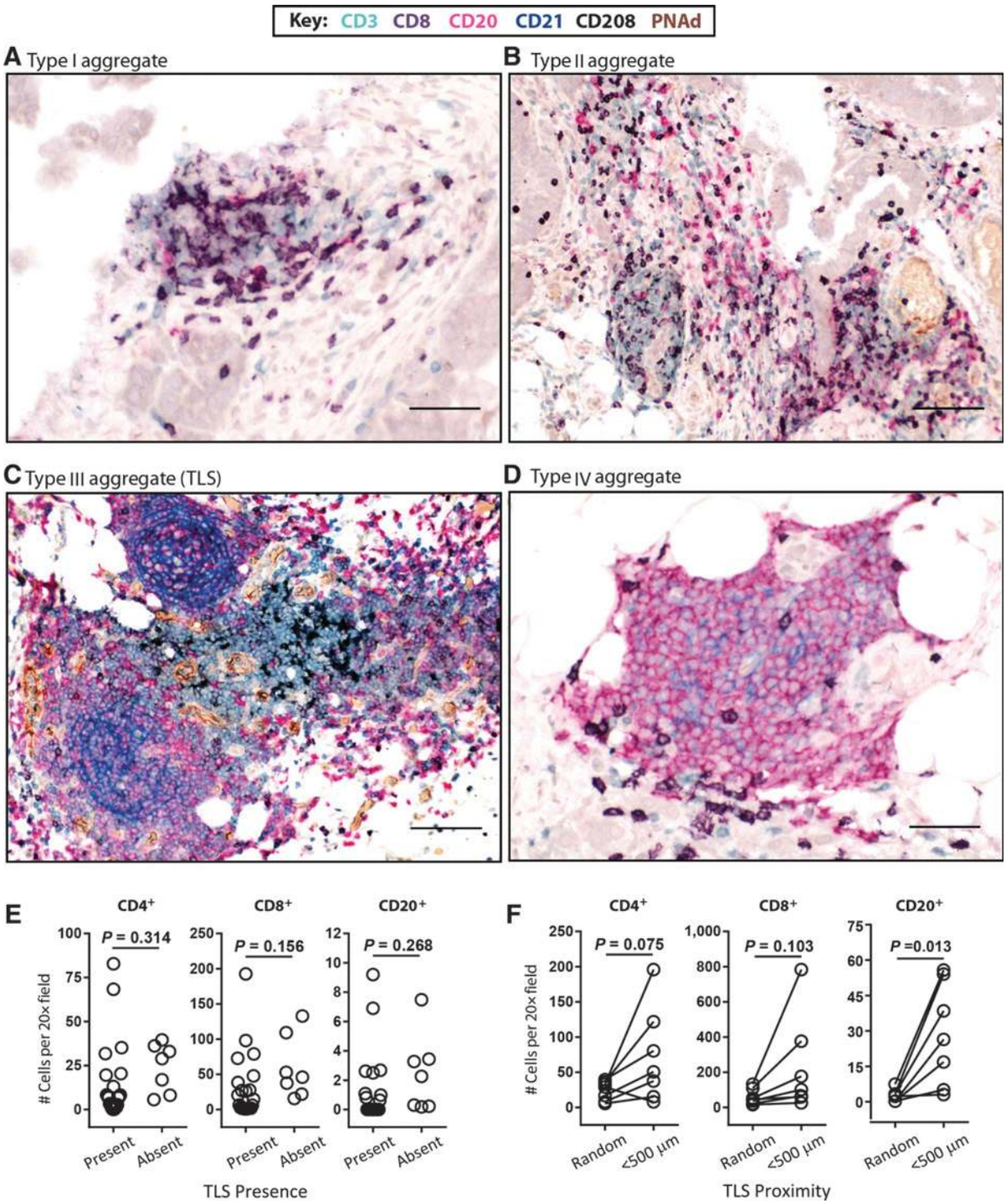

Figure 1.
Six-color IHC reveals four types of lymphoid aggregates in HGSC and associations with TIL. Antibodies to CD3 (green), CD8 (purple), CD20 (red), CD21 (blue), CD208 (black), and PNAd (brown) were used to visualize lymphoid aggregates in whole tumor sections from 30 HGSC cases. A, type I aggregates contained $CD8^+$ T cells, $CD4^+$ T cells (detected as $CD3^+CD8^-$ cells), $CD20^+$ B cells, and $CD208^+$ DCs. B, type II aggregates contained $CD8^+$ T cells, $CD4^+$ T cells, and $CD20^+$ B cells in diffuse patterns with no clear follicles or T-cell zones. C, type III aggregates (TLS) contained B-cell follicles with GCs distinguished by interdigitating networks of $CD21^+$ fDCs. B-cell follicles were adjacent to T-cell zones containing primarily $CD4^+$ T cells and $CD208^+$ DCs, as well as $CD8^+$ T cells. $PNAd^+$ vessels were found in T-cell zones and surrounding follicles. D, type IV aggregates contained $CD20^+$ B cells and $CD21^+$ fDCs without clear T-cell zones and may represent milky spots. E, densities of $CD4^+$, $CD8^+$, and $CD20^+$ TIL in tumors in which TLSs were present ($n = 7$) or absent ($n = 23$). F, mean densities of $CD4^+$, $CD8^+$, and $CD20^+$ TIL in 10 random fields versus 10 fields within 500 μm of a TLS center ($n = 7$ cases). *P* values refer to means that were compared using unpaired (E) or paired (F) *t* tests. Scale bars: A and D = 50 μm; B and C=100 μm.

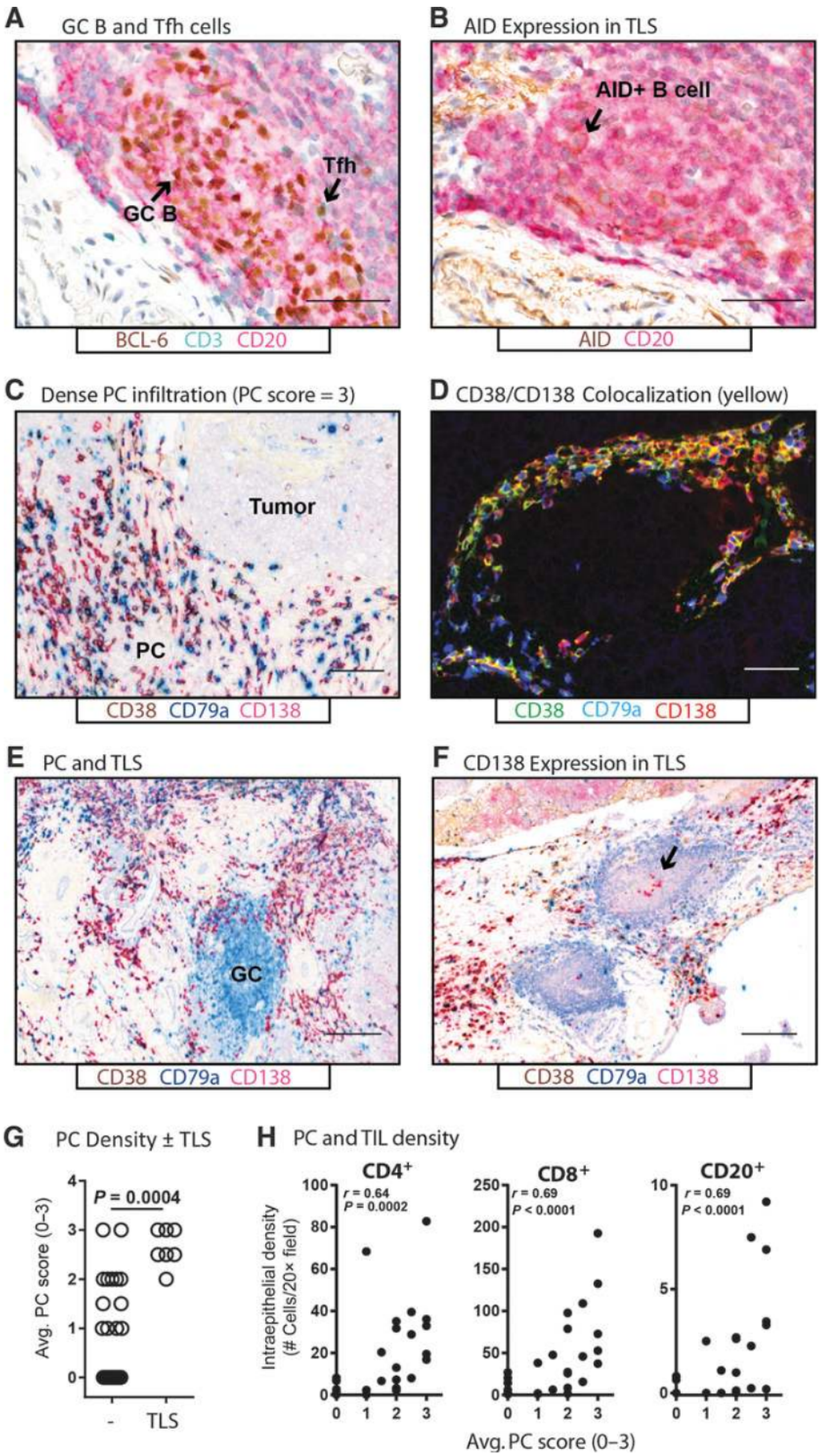

Figure 2.
Evidence of ongoing immune reactions within TLS in HGSC. TLS were analyzed by multicolor IHC for various immune-related markers. A, three-color stain for BCL-6 (brown), CD3 (green), and CD20 (red) showing BCL-6$^+$ B cells and Tfh in a GC. B, two-color stain for AID (brown) and CD20 (red) showing AID$^+$ B cells in a GC. C, three-color stain for CD38 (brown), CD79a (blue), and CD138 (red) showing dense stromal infiltration by PCs (PC score = 3). D, false-colored image of PCs showing colocalization of CD38 (green) and CD138 (red) (merge = yellow). E, example of a TLS surrounded by PCs. F, CD138$^+$ cells (arrow) within a TLS-associated GC, possibly representing an early stage of PC differentiation. G, average stromal density of PCs (on a scale of 0–3) in tumors without ($n = 23$) and with ($n = 7$) TLS. *P* value, Mann–Whitney test. H, association between stromal PC scores and the average density of CD4$^+$, CD8$^+$, and CD20$^+$ TIL. *r* and *P* values refer to Spearmann correlation. Scale bars: A, B, and D = 50 μm; C = 100 μm; E and F = 200 μm.

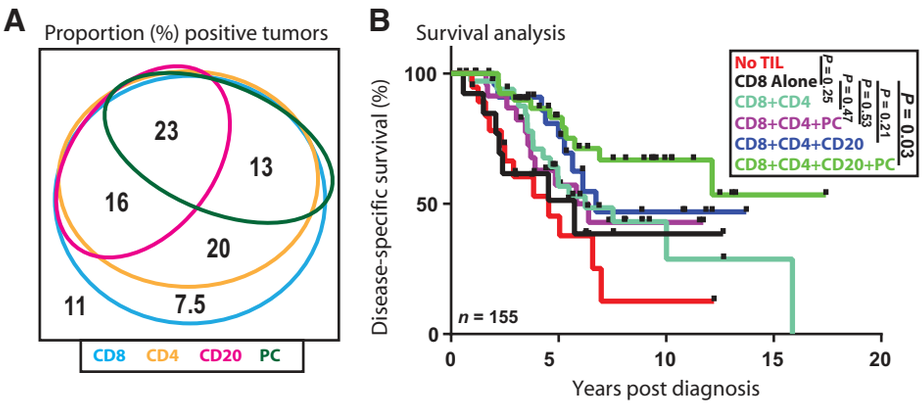

Figure 3.
Relationship between PCs, TIL subsets, and patient survival. A, Venn diagram showing the interrelationships between TIL subsets in the 172-case HGSC TMA. Colored circles indicate patient subgroups that were positive for the indicated TIL subsets: blue = CD8, orange = CD4, pink = CD20, green = PCs. Numbers indicate the proportion (%) of cases in each subgroup. B, Kaplan–Meier analysis of disease-specific survival for six patient subgroups based on the indicated TIL patterns. *P* values refer to log rank tests between the indicated groups.

basis of the surface expression of IgD and CD38, we identified three major $CD19^+$ lymphocyte subsets: $IgD^+IgG^-CD38^-$ naïve B cells, $IgD^-IgG^+CD38^-$ memory B cells, and $IgD^-IgG^+CD38^+$ PCs (Fig. 4A). As shown previously (11), the majority of memory B cells were IgG positive (Fig. 4B). PCs comprised from 5% to 88% of $CD19^+$ cells and also expressed surface IgG (Fig. 4B). As in the immunohistochemical analysis, there was a trend toward larger proportions of PCs in tumors containing TLS (mean proportion of $CD19^+$ cells: 39% vs. 25%), although 2 of 12 tumors had abundant PCs (>30% of $CD19^+$ cells) despite lacking TLS.

$CD19^+$ cells were further assessed for expression of B-cell differentiation markers. As expected, naïve B cells were $CD20^+CD27^-CD95^-CD138^-$, and memory B cells were $CD20^+CD27^+CD95^+CD138^-$ (Fig. 4C). Also as expected, PCs were $CD20^-CD27^+CD95^+$ and showed low but consistent expression of CD138 (Fig. 4C). The chemokine receptors CXCR5 and CXCR3 recruit B-lineage cells into follicles and sites of inflammation, respectively. As expected, naïve B cells expressed CXCR5 but not CXCR3, whereas the memory B-cell population was a mixture of $CXCR5^+$ and $CXCR3^+$ cells (Fig. 4C). In contrast, PCs universally expressed CXCR3, but not CXCR5. Thus, PCs appeared to be at an early stage of differentiation and had an inflammatory chemokine receptor profile.

To assess clonality, we FACS-purified PCs from 3 tumors and sequenced the immunoglobulin heavy-chain variable regions. Bulk tumor samples and FACS-purified memory B cells were analyzed for comparison. In 3 of 3 tumors, PC-derived sequences were restricted to 10 to 28 distinct *VDJ* families (Fig. 4D, Supplementary Table S1), suggesting a high degree of clonal expansion. There was also widespread evidence of somatic hypermutation within *VDJ* families, with most sequences showing at least 5% divergence from germline. Although CDR3 sequences from PCs and memory B cells showed some overlap, PC-derived sequences were most similar to those from bulk tumor in terms of both diversity and prevalence (Fig. 4D). Thus, PCs were clonally expanded and represented the predominant source of IgG mRNA in tumors.

Identification of a minimal plasma cell gene expression signature

To investigate the relationship between PCs and the underlying molecular and genetic features of HGSC, we sought to identify a PC-associated gene expression signature that could be used to interrogate the TCGA dataset. We assessed the expression of 770 cancer/immune–related genes in 19 HGSC samples that, in the above immunohistochemical analyses, were found to be (i) positive for both PCs and $CD20^+$ B cells ($n = 10$), (ii) positive for PCs but negative for $CD20^+$ B cells ($n = 4$), (iii) negative for PCs but positive for $CD20^+$ B cells ($n = 2$), and (iv) negative for both PCs and $CD20^+$ B cells ($n = 3$). All tumors contained $CD4^+$ and $CD8^+$ TIL. Average transcript counts between the 4 subgroups were highly concordant (Fig 5A; Pearson $r^2 > 0.85$). However, 66 genes were expressed at >10-fold higher levels in PC high tumors (PC score of 3; $n = 4$; Supplementary Table S2), including the B-lineage genes *CD79A*, *MS4A1* (CD20), and *TNFRSF17* (B-cell maturation antigen; BCMA; Fig. 5A). Of these, expression of *TNFRSF17* was uniquely associated with PC-positive tumors compared with tumors containing B cells but not PCs, or the other subgroups of tumors (Supplementary Table S2). TNFRSF17/BCMA is known to be expressed when B cells differentiate into antibody-secreting cells (24), and it is essential for the survival of long-lived PCs, but not memory B cells (25). Moreover, *TNFRSF17* has been described as a signature gene for human PCs (26).

Given our observation that PCs contribute the majority of IgG mRNA in HGSC tumors (Fig. 3D), we reasoned that *TNFRSF17* and IgG gene expression levels should be correlated. Indeed, analysis of microarray data from 570 untreated HGSC tumor specimens in the TCGA dataset (27) revealed a strong correlation between the expression of *TNFRSF17* and the immunoglobulin-joining region (*IGJ*) gene segment, which is common to all antibody mRNA transcripts (Spearman $r = 0.86$; Pearson $r^2 = 0.81$). When we plotted normalized gene expression values for these two genes, three patient subgroups emerged (Fig. 5B): (i) high expression of both *TNFRSF17* and *IGJ* ($n = 56$), (ii) moderate to high expression of *IGJ* but not *TNFRSF17* ($n = 313$), and (iii) negligible expression of *TNFRSF17* and *IGJ* ($n = 201$). A similar pattern was seen using RNA-seq data from a subset of these tumors (Fig. 5C). As expected, tumors that expressed both *TNFRSF17* and *IGJ* also expressed high levels of *IGHV* segments (Fig. 5D). The majority of such cases expressed 5 to 15 *IGHV* segments (Fig. 5D), consistent with the oligoclonal nature of IgG transcripts previously observed by Sanger sequencing of *IGHV* regions (Fig. 4D). Finally, in accord with our flow cytometry data (Fig. 4B), IgG-derived transcripts were far more abundant than other immunoglobulin subtypes. Specifically, *IGG1*, *IGG2*, and *IGG3* were predominant, with low expression of *IGG4*, *IGA1*, and *IGM* in some cases (Supplementary Fig. S1). Thus, *TNFRSF17* and *IGJ* comprised a 2-gene signature that distinguished TCGA cases with

(i) both PCs and CD20$^+$ TIL (*TNFRSF17*^{high} and *IGJ*^{high}); (ii) CD20$^+$ TIL without PCs (*TNFRSF17*^{low} and *IGJ*^{high}); and (iii) neither CD20$^+$ TIL nor PCs (*TNFRSF17*^{low} and *IGJ*^{low}).

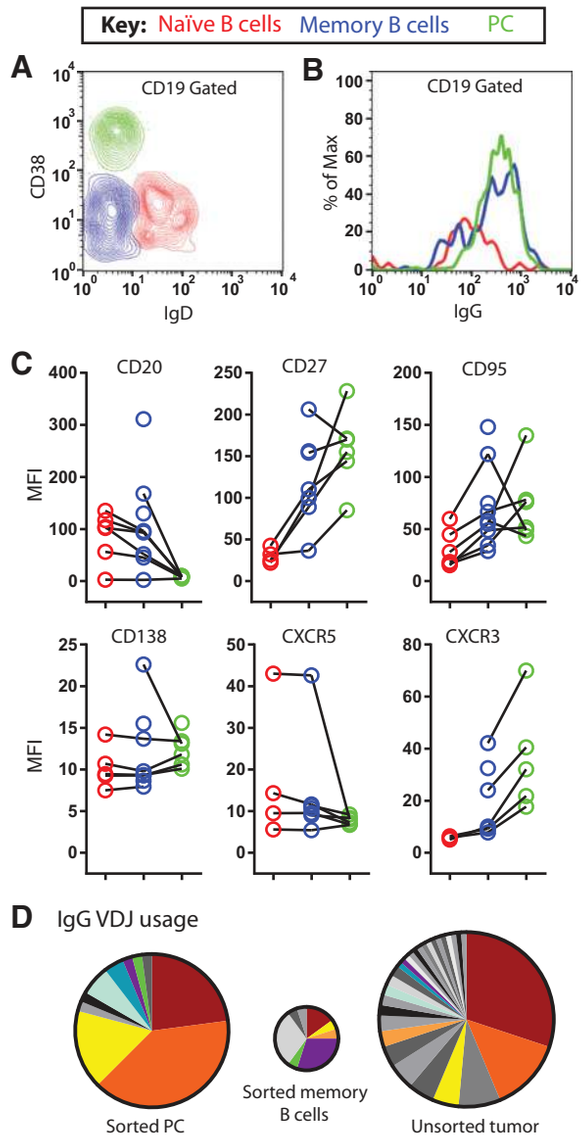

Figure 4.
Cell surface phenotypes and clonality of B-lineage cells in HGSC. A–C, multicolor flow cytometry was used to analyze TIL from 12 disaggregated tumor samples. Data are color coded as follows: red = naïve B cells (IgD$^+$, CD38$^-$), blue = memory B cells (IgD$^-$, CD38$^-$), and green = PCs (IgD$^-$, CD38hi). A, representative contour plot showing expression of IgD and CD38 on CD19$^+$ cells. B, IgG expression on CD19$^+$ cells. C, expression levels (mean fluorescence intensity, MFI) of the indicated cell surface markers on CD19$^+$ cells from a subset of tumor samples. The same color-coding scheme is used as in A and B. D, diversity and sharing of immunoglobulin variable regions from PCs, memory B cells, and bulk tumor tissue from a representative HGSC case. The overall size of each pie indicates the relative number of unique productive IgG sequences observed in each sample. The size of each pie slice indicates the relative abundance of each VDJ rearrangement within a sample. VDJ rearrangements that were found in more than one sample are colored to show the pattern of sharing between samples. VDJ rearrangements that were found in only one sample are shown on a gray scale. Similar results were seen with two other HGSC cases.

Association of the PC signature with immune-related genes, patient survival, and cancer–testis antigens

The *TNFRSF17*/*IGJ* gene signature was used to explore associations between PCs and other immune-related gene products in the TCGA gene expression microarray dataset. Consistent with our IHC data (Fig. 2E), tumors with a PC signature (i.e., *TNFRSF17*^{high} and *IGJ*^{high}) showed elevated expression of *CXCL13* (which contributes to the establishment and organization of TLS) and *IL21* (which is produced primarily by Tfh cells; Fig. 6A). Although a marker of TLS, CXCL13 is unlikely to serve as a chemoattractant for PCs, as PCs express the inflammation-associated chemokine receptor CXCR3 rather than CXCR5 (Fig. 4C; ref. 28). Indeed, the three CXCR3 ligands (*CXCL9*, *CXCL10*, and *CXCL11*) were highly expressed in tumors with PC or B-cell signatures (Fig. 6B), providing a plausible mechanism for attraction of PCs to the tumor microenvironment. Tumors with a PC signature also showed high expression of *TNFSF13B* (BAFF, a ligand for BCMA; Fig. 6C). In contrast, *IL6* levels were only modestly elevated, and *TNFSF13* (APRIL) and *CXCL12* levels were similar to the PC-negative subgroups (Fig. 6C). Thus, the BAFF/BCMA axis might provide the primary growth and survival signal for PCs in the HGSC microenvironment.

We also evaluated the relationship between PCs, cytolytic gene signatures, and prognosis. Consistent with our IHC data (Fig. 2H), we observed a stepwise increase in the expression of *CD8A* (a marker of CD8$^+$ TIL) in cases with B-cell and PC signatures (Fig. 6D), whereas expression of the Treg-associated transcription factor *FOXP3* was uniform across subgroups (Fig. 6E). Cases with the PC gene signature also showed elevated expression of *IFNG*, *GZMB*, and *PRF1* (Fig. 6F). The PC gene signature was strongly associated with overall survival (no B cells vs. PC, log rank $P = 0.0086$; B cells vs. PC $P = 0.0241$), whereas *IGJ* alone carried no prognostic benefit (Fig. 6G). Thus, consistent with our IHC data (Fig. 3B), PCs were associated with cytotoxic immune responses and patient survival.

To gain insight into potential target antigens of PCs, we evaluated the relationship between the PC gene signature and various classes of tumor antigen. Nonsynonymous point mutations can give rise to "neo-epitopes" that are recognized by CD8$^+$ and CD4$^+$ TIL (29). However, neither the PC nor B-cell gene signatures showed an association with the total number of point mutations in tumors ($\chi^2P = 0.9429$; Fig. 6H) nor predicted HLA-A associated neoepitopes ($\chi^2P = 0.7675$; Supplementary Fig. S2A). Although *BRCA1* impairment has been correlated with the expression of TIL-related genes in HGSC (30,31), the PC and B-cell gene signatures showed no association with *BRCA1* impairment (including germline mutations, somatic mutations, and DNA methylation; $\chi^2P = 0.7415$; Fig. 6I) nor *BRCA2* mutation ($\chi^2P = 0.9142$). Likewise, the PC and B-cell gene signatures were not associated with specific types of *TP53* mutation ($\chi^2P = 0.7175$; Supplementary Fig. S2B). We also evaluated the expression of 45 commonly overexpressed antigens and 15 well-characterized differentiation antigens (Supplementary Table S3) but found no association with the PC or B-cell gene signatures (Supplementary Fig. S2C). Finally, we assessed the expression of 104 cancer–testis (CT) antigens. Tumors with a PC signature expressed 2-fold more CT antigens on average than tumors with a B-cell signature or no B-cell signature (cutoff: $z = 3$, ANOVA $P = 0.0003$; Fig. 6J). Similar results were obtained using different thresholds for gene expression ($z = 2$, $P = 0.0093$ and $z = 4$, $P < 0.0001$). Semisupervised hierarchical clustering revealed a subset of CT antigens that were

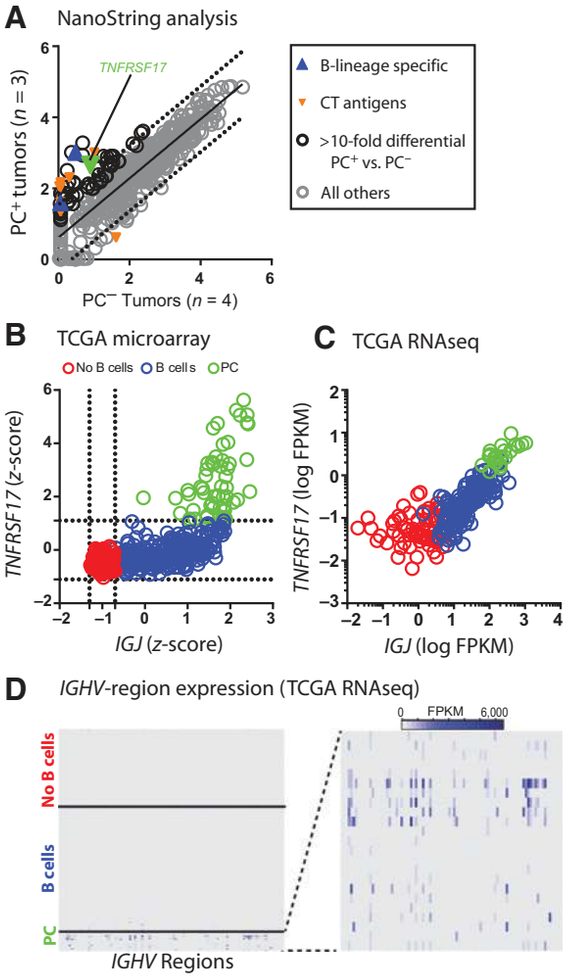

Figure 5.
Gene expression analysis reveals a 2-gene PC signature. A, NanoString gene expression analysis comparing $\log_{10}$ average gene counts from tumors containing no PC infiltrates ($n = 4$) to those with heavy PC infiltrates ($n = 3$). Highlighted genes are those expressed at a greater than 10-fold differential between groups. B, standardized microarray gene expression values (*z*-scores) for *IGJ* versus *TNFRSF17* from TCGA Affymetrix U133HT GeneChip data showing three distinct patient subgroups ($n = 570$). C, standardized read-count data (fragments per kilobase per million reads; FPKM) for *IGJ* and *TNFRSF17* from the TCGA RNA-seq dataset ($n = 273$). Data points are colored based on calls from microarray data (B). D, *IGHV* region expression (FPKM) in TCGA cases exhibiting the *TNFRSF17*/*IGJ* PC signature, the *IGJ* B-cell signature, or no B-cell signature. The right panel shows an expanded view of *IGHV* regions from PC signature–positive cases.

overrepresented in cases with a PC gene signature (Supplementary Fig. S3), including known targets of autoantibody responses such as NY-ESO-1, MAGEA1, and CTAG2 (Supplementary Fig. S3; Supplementary Table S4). Thus, from this broad bioinformatic analysis, CT antigens emerged as a potential class of target antigen underlying PC responses in HGSC.

Discussion

While investigating lymphoid aggregates in HGSC, we discovered a novel, prognostically significant association between TIL, TLS, and PCs. PCs were strongly associated with mature TLS and formed dense aggregates in tumor stroma. PCs had an early-differentiated phenotype, expressed surface IgG, and showed evidence of clonal expansion and somatic hypermutation. PC infiltrates were strongly associated with $CD8^+$ TIL and other hallmarks of cytotoxic immune responses. Indeed, $CD8^+$ TIL carried prognostic benefit only when found in combination with PCs, $CD20^+$ TIL, and $CD4^+$ TIL, suggesting these four lymphocyte subsets work in concert to promote antitumor immunity. Interrogation of the TCGA dataset revealed correlations between PCs and other features of active antitumor responses, including B-lymphoid growth and survival factors, TLS-associated genes, and cytokines and chemokines associated with cytolytic immune responses. Tumors with a PC gene signature had average mutation loads and *BRCA1/2* status but expressed more CT antigens, suggesting the latter represent target antigens for PC responses. Collectively, our findings reveal an important but underappreciated collaboration between PCs and TIL in antitumor immunity. With better understanding, it may be possible to enhance these functional interactions to achieve improved tumor surveillance and more durable responses to immunotherapy.

The positive associations we found between PCs and tumor immunity are consistent with some, but not all, prior reports concerning the immunologic role of PCs. On the positive side, PCs or PC-like gene signatures have been associated with favorable prognosis in breast (14), lung (21), colorectal (12), and other cancers (13). Indeed, in a recent pan-cancer gene expression analysis, a PC-associated gene signature was among the strongest positive prognostic factors across cancer types (26). Moreover, prognostically favorable "B-cell" gene signatures often contain immunoglobulin transcripts (14,32), which our data indicate are likely attributable to PCs (Fig. 4D). On the other hand, both B cells (33,34) and PCs have been shown to play inhibitory roles in cancer and other settings. Recent studies in infection and autoimmunity have identified a subset of PCs ("regulatory" PCs) that inhibit T-cell responses via the immunosuppressive cytokines IL10 and IL35 (35). Shalapour and colleagues recently described a similar PC subset in murine and human prostate cancer that inhibited $CD8^+$ T cell–mediated tumor immunity and consequently the effectiveness of chemotherapy (36). Notably, this PC subset expressed IgA, IL10, and PD-L1 and differentiated in response to TGFβ. In contrast, we found that PCs in HGSC universally expressed IgG (Fig. 4B and Supplementary Fig. S1), suggesting they undergo class switching in a proimmune milieu dominated by cytokines such as IFNγ rather than TGFβ. Moreover, HGSC-associated PCs expressed CXCR3 (Fig. 4C), which is induced in B-lineage cells by an IFNγ/T-bet dependent pathway and enables their recruitment to inflammatory sites (37). $CXCR3^+$ PCs have also been described in autoimmunity, where they serve to exacerbate rather than suppress immune responses (38,39). Thus, the immunosuppressive PCs described in prostate cancer (36) may be unique to that disease, as the PCs found in HGSC and other malignancies have properties and associations consistent with a positive role in antitumor immunity.

Given the strong prognostic significance of $CD8^+$ TIL, it is widely assumed that they are the primary mediators of antitumor immunity. However, $CD8^+$ TILs are often functionally impaired in the tumor microenvironment (40), raising the possibility that alternative immune mechanisms are equally, if not more, important. As the normal physiologic role of PCs is to serve as "antibody factories", they could mediate antitumor effects by producing antibodies against tumor-associated antigens. Such effects might

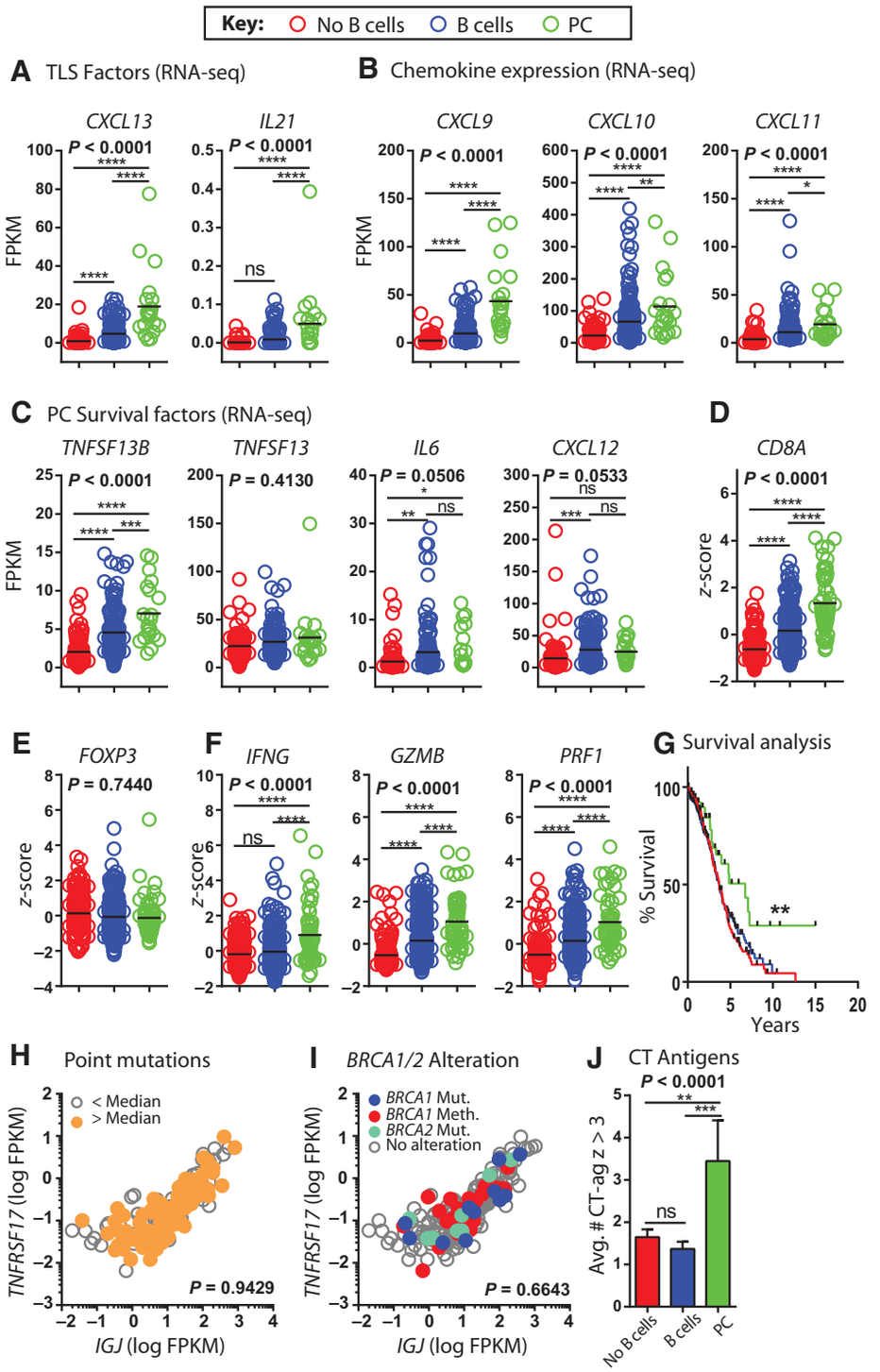

Figure 6.
The PC gene signature is associated with markers of active humoral and cellular immunity, patient survival, and CT antigen expression. As in Fig. 5, TCGA cases were stratified into three groups based on the expression of *IGJ* and *TNFRSF17*: red = no B-cell signature, blue = B-cell signature, and green = PC signature. A, expression of TLS-associated factors. B, expression of chemokine ligands for CXCR3. C, expression of PC survival factors. D, expression of *CD8A*, an indicator of $CD8^+$ TIL. E, expression of *FOXP3*. F, expression of cytotoxicity-associated gene products. A–F, *P* values refer to one-way ANOVA with Tukey *post hoc* comparison. *, $P < 0.05$; ***, $P < 0.001$; ****, $P < 0.0001$. G, Kaplan–Meier survival analysis of HGSC cases from the TCGA dataset ($n = 570$). **, log rank tests between indicated groups: no B cells versus PC $P = 0.0086$, B cells versus PC $P = 0.0241$. H, TCGA RNA-seq normalized gene expression values for *IGJ* and *TNFRSF17* were overlaid with calls for above median levels of nonsynonymous point mutations ($n = 219$). *P* value, χ^2 test. I, analysis was performed as in A but overlaid with *BRCA1* alterations (including germline and somatic mutations and promotor methylation) and *BRCA2* mutations (germline and somatic; $n = 316$). *P* value, χ^2 test. J, average numbers of expressed CT antigens (TCGA microarray gene expression values > 3 SDs above the mean) in cases with no B-cell signature, the B-cell signature, or the PC signature ($n = 570$). *P* value, one-way ANOVA with Tukey *post hoc* comparisons; **, $P < 0.01$; ***, $P < 0.0001$.

be augmented by the dense localization of PCs in tumor stroma, which would enable high concentrations of antibody to accumulate locally. Theoretically, PC-derived antibodies could mediate direct antitumor effects by binding to and disrupting the function of their cognate antigens, activating the complement pathway, and/or triggering antibody-dependent cellular cytotoxicity (ADCC; ref. 41). In this regard, the predominant antibody subtypes in HGSC included IgG1 and IgG3 (Supplementary Fig. S1), which can activate both complement and ADCC (41). Finally, PC-derived antibodies could opsonize tumor antigens, thereby facilitating antigen presentation and broadening of T-cell responses (42).

Defining the antitumor mechanisms used by PCs will require identification of their cognate antigens. Our TCGA analyses

suggest that PC-derived antibodies preferentially recognize CT antigens over differentiation/overexpressed antigens or mutant gene products (Fig. 6 and Supplementary Fig. S2). Of the 31 CT antigens that were associated with PC signature–positive tumors (Supplementary Table S4), 27 (87%) are encoded on the X chromosome (CT-X antigens). Given that CT-X antigens represent only about 50% of all known or predicted CT antigens (http://www.cta.lncc.br/), this represents a marked overrepresentation of CT-X antigens in PC-positive tumors. In agreement with our findings, Germain and colleagues recently demonstrated recognition of multiple CT-X antigens by tumor-associated antibodies in lung cancer (43). Thus, aberrant expression of X chromosome genes might be a general mechanism for inducing PC responses in cancer. Other classes of antigen might also be relevant, as lung cancer–derived antibodies have also been shown to recognize p53 and various overexpressed self-antigens (44). Furthermore, antibodies derived from medullary breast cancer were shown to recognize ganglioside D3 and an apoptosis-associated form of actin (45,46).

In addition to antibodies, PCs could influence antitumor immunity through cell-based mechanisms. PCs can regulate T-cell responses by expressing cytokines and other immunomodulatory factors (35). Another possibility is that PCs might physically exclude immune-suppressive cell types, such as cancer-associated fibroblasts and myeloid-derived suppressor cells (47), creating a more permissive tumor microenvironment for $CD8^+$ TIL responses. Indeed, lymphocyte- and mesenchymal-derived gene signatures are inversely correlated in HGSC (4,30).

Our findings suggest several novel avenues for cancer immunotherapy. The antibody-mediated effects of PCs could potentially be mimicked through administration of recombinant antibodies combined with immune modulators that enhance downstream processes such as antigen spreading, CDC and ADCC. The cell-mediated effects of PCs could potentially be reproduced by adoptive transfer of tumor-specific PCs, induction of TLS using vectors that express relevant cytokines/chemokines (48), or therapeutic vaccination (49,50). By designing immunotherapies that engage both the humoral and cellular arms of the immune system, it should be possible to establish endogenous tumor surveillance mechanisms that more effectively contend with the spatial heterogeneity and continual evolution of advanced cancers.

Disclosure of Potential Conflicts of Interest

No potential conflicts of interest were disclosed.

Authors' Contributions

Conception and design: D.R. Kroeger, K. Milne, B.H. Nelson
Development of methodology: D.R. Kroeger, K. Milne
Acquisition of data (provided animals, acquired and managed patients, provided facilities, etc.): D.R. Kroeger, K. Milne, B.H. Nelson
Analysis and interpretation of data (e.g., statistical analysis, biostatistics, computational analysis): D.R. Kroeger, B.H. Nelson
Writing, review, and/or revision of the manuscript: D.R. Kroeger, K. Milne, B.H. Nelson
Administrative, technical, or material support (i.e., reporting or organizing data, constructing databases): K. Milne
Study supervision: B.H. Nelson

Acknowledgments

The authors thank Michael Anglesio, Scott Brown, and Rob Holt for advice and assistance.

Grant Support

This study was supported by Canadian Institutes of Health Research (Award MOP-137133), U.S. Department of Defense (Award W81XWH-12-1-0604), Canadian Cancer Society Research Institute (Award 702497), OVCARE & Vancouver General Hospital Foundation (Carraressi Foundation Research Grant, 2013), and BC Cancer Foundation.

The costs of publication of this article were defrayed in part by the payment of page charges. This article must therefore be hereby marked *advertisement* in accordance with 18 U.S.C. Section 1734 solely to indicate this fact.

Received November 12, 2015; revised January 5, 2016; accepted January 7, 2016; published OnlineFirst January 13, 2016.

References

1. Tabassum DP, Polyak K. Tumorigenesis: it takes a village. Nat Rev Cancer 2015;15:473–83.
2. Pribluda A, de la Cruz CC, Jackson EL. Intratumoral heterogeneity: from diversity comes resistance. Clin Cancer Res 2015;21:2916–23.
3. Bowtell DD, Bohm S, Ahmed AA, Aspuria PJ, Bast RCJr, Beral V, et al. Rethinking ovarian cancer II: reducing mortality from high-grade serous ovarian cancer. Nat Rev Cancer 2015;15:668–79.
4. The Cancer Genome Atlas Network. Integrated genomic analyses of ovarian carcinoma. Nature 2011;474:609–15.
5. Bashashati A, Ha G, Tone A, Ding J, Prentice LM, Roth A, et al.Distinct evolutionary trajectories of primary high-grade serous ovarian cancers revealed through spatial mutational profiling. J Pathol 2013;231:21–34.
6. Schwarz RF, Ng CK, Cooke SL, Newman S, Temple J, Piskorz AM, et al. Spatial and temporal heterogeneity in high-grade serous ovarian cancer: a phylogenetic analysis. PLoS Med 2015;12:e1001789.
7. Patch AM, Christie EL, Etemadmoghadam D, Garsed DW, George J, Fereday S, et al.Whole-genome characterization of chemoresistant ovarian cancer. Nature 2015;521:489–94.
8. Castellarin M, Milne K, Zeng T, Tse K, Mayo M, Zhao Y, et al.Clonal evolution of high-grade serous ovarian carcinoma from primary to recurrent disease. J Pathol 2013;229:515–24.
9. Hwang WT, Adams SF, Tahirovic E, Hagemann IS, Coukos G. Prognostic significance of tumor-infiltrating T cells in ovarian cancer: a meta-analysis. Gynecol Oncol 2012;124:192–8.
10. Milne K, Kobel M, Kalloger SE, Barnes RO, Gao D, Gilks CB, et al.Systematic analysis of immune infiltrates in high-grade serous ovarian cancer reveals CD20, FoxP3 and TIA-1 as positive prognostic factors. PLoS One 2009;4:e6412.
11. Nielsen JS, Sahota RA, Milne K, Kost SE, Nesslinger NJ, Watson PH, et al. CD20+ tumor-infiltrating lymphocytes have an atypical CD27- memory phenotype and together with CD8+T cells promote favorable prognosis in ovarian cancer. Clin Cancer Res 2012;18:3281–92.
12. Richards CH, Flegg KM, Roxburgh CS, Going JJ, Mohammed Z, Horgan PG, et al.The relationships between cellular components of the peritumoural inflammatory response, clinicopathological characteristics and survival in patients with primary operable colorectal cancer. Br J Cancer 2012;106:2010–5.
13. Schmidt M, Hellwig B, Hammad S, Othman A, Lohr M, Chen Z, et al.A comprehensive analysis of human gene expression profiles identifies stromal immunoglobulin kappa C as a compatible prognostic marker in human solid tumors. Clin Cancer Res 2012;18:2695–703.
14. Iglesia MD, Vincent BG, Parker JS, Hoadley KA, Carey LA, Perou CM, et al.Prognostic B-cell signatures using mRNA-seq in patients with subtype-specific breast and ovarian cancer. Clin Cancer Res 2014;20:3818–29.
15. Yanni G, Whelan A, Feighery C, Bresnihan B. Analysis of cell populations in rheumatoid arthritis synovial tissues. Semin Arthritis Rheum 1992;21:393–9.

16. Pitzalis C, Jones GW, Bombardieri M, Jones SA. Ectopic lymphoid-like structures in infection, cancer and autoimmunity. Nat Rev Immunol 2014;14:447–62.
17. Dieu-Nosjean MC, Antoine M, Danel C, Heudes D, Wislez M, Poulot V, et al.Long-term survival for patients with non-small-cell lung cancer with intratumoral lymphoid structures. J Clin Oncol 2008;26:4410–7.
18. Martinet L, Garrido I, Filleron T, Le Guellec S, Bellard E, Fournie JJ, et al. Human solid tumors contain high endothelial venules: association with T- and B-lymphocyte infiltration and favorable prognosis in breast cancer. Cancer Res 2011;71:5678–87.
19. Coppola D, Nebozhyn M, Khalil F, Dai H, Yeatman T, Loboda A, et al. Unique ectopic lymph node-like structures present in human primary colorectal carcinoma are identified by immune gene array profiling. Am J Pathol 2011;179:37–45.
20. Clarke B, Tinker AV, Lee CH, Subramanian S, van de Rijn M, Turbin D, et al.Intraepithelial T cells and prognosis in ovarian carcinoma: novel associations with stage, tumor type, and BRCA1 loss. Mod Pathol 2009;22:393–402.
21. Lohr M, Edlund K, Botling J, Hammad S, Hellwig B, Othman A, et al.The prognostic relevance of tumour-infiltrating plasma cells and immunoglobulin kappa C indicates an important role of the humoral immune response in non-small cell lung cancer. Cancer Lett 2013;333: 222–8.
22. Rangel-Moreno J, Moyron-Quiroz JE, Carragher DM, Kusser K, Hartson L, Moquin A, et al.Omental milky spots develop in the absence of lymphoid tissue-inducer cells and support B and T cell responses to peritoneal antigens. Immunity 2009;30:731–43.
23. deLeeuw RJ, Kroeger DR, Kost SE, Chang PP, Webb JR, Nelson BH. CD25 Identifies a Subset of CD4+FoxP3− TIL That Are Exhausted Yet Prognostically Favorable in Human Ovarian Cancer. Cancer Immunol Res 2015;3:245–53.
24. Darce JR, Arendt BK, Wu X, Jelinek DF. Regulated expression of BAFF-binding receptors during human B cell differentiation. J Immunol 2007;179:7276–86.
25. O'Connor BP, Raman VS, Erickson LD, Cook WJ, Weaver LK, Ahonen C, et al.BCMA is essential for the survival of long-lived bone marrow plasma cells. J Exp Med 2004;199:91–8.
26. Gentles AJ, Newman AM, Liu CL, Bratman SV, Feng W, Kim D, et al.The prognostic landscape of genes and infiltrating immune cells across human cancers. Nat Med 2015;21:938–45.
27. Cerami E, Gao J, Dogrusoz U, Gross BE, Sumer SO, Aksoy BA, et al.The cBio cancer genomics portal: an open platform for exploring multidimensional cancer genomics data. Cancer Discov 2012;2:401–4.
28. Kunkel EJ, Butcher EC. Plasma-cell homing. Nat Rev Immunol 2003; 3:822–9.
29. Schumacher TN, Schreiber RD. Neoantigens in cancer immunotherapy. Science 2015;348:69–74.
30. Tothill RW, Tinker AV, George J, Brown R, Fox SB, Lade S, et al.Novel molecular subtypes of serous and endometrioid ovarian cancer linked to clinical outcome. Clin Cancer Res 2008;14:5198–208.
31. George J, Alsop K, Etemadmoghadam D, Hondow H, Mikeska T, Dobrovic A, et al.Nonequivalent gene expression and copy number alterations in high-grade serous ovarian cancers with BRCA1 and BRCA2 mutations. Clin Cancer Res 2013;19:3474–84.
32. Bindea G, Mlecnik B, Tosolini M, Kirilovsky A, Waldner M, Obenauf AC, et al.Spatiotemporal dynamics of intratumoral immune cells reveal the immune landscape in human cancer. Immunity 2013;39:782–95.
33. Qin Z, Richter G, Schuler T, Ibe S, Cao X, Blankenstein T. B cells inhibit induction of T cell-dependent tumor immunity. Nat Med 1998;4:627–30.
34. Olkhanud PB, Damdinsuren B, Bodogai M, Gress RE, Sen R, Wejksza K, et al.Tumor-evoked regulatory B cells promote breast cancer metastasis by converting resting CD4(+) T cells to T-regulatory cells. Cancer Res 2011;71:3505–15.
35. Fillatreau S.Regulatory plasma cells. Curr Opin Pharmacol 2015;23:1–5.
36. Shalapour S, Font-Burgada J, Di Caro G, Zhong Z, Sanchez-Lopez E, Dhar D, et al.Immunosuppressive plasma cells impede T-cell-dependent immunogenic chemotherapy. Nature 2015;521:94–8.
37. Muehlinghaus G, Cigliano L, Huehn S, Peddinghaus A, Leyendeckers H, Hauser AE, et al.Regulation of CXCR3 and CXCR4 expression during terminal differentiation of memory B cells into plasma cells. Blood 2005;105:3965–71.
38. Lacotte S, Decossas M, Le Coz C, Brun S, Muller S, Dumortier H. Early differentiated CD138(high) MHCII+ IgG+ plasma cells express CXCR3 and localize into inflamed kidneys of lupus mice. PLoS One 2013;8: e58140.
39. Chihara N, Aranami T, Oki S, Matsuoka T, Nakamura M, Kishida H, et al. Plasmablasts as migratory IgG-producing cells in the pathogenesis of neuromyelitis optica. PLoS One 2013;8:e83036.
40. Jiang Y, Li Y, Zhu B. T-cell exhaustion in the tumor microenvironment. Cell Death Dis 2015;6:e1792.
41. Vidarsson G, Dekkers G, Rispens T. IgG subclasses and allotypes: from structure to effector functions. Front Immunol 2014;5:520.
42. Carmi Y, Spitzer MH, Linde IL, Burt BM, Prestwood TR, Perlman N, et al. Allogeneic IgG combined with dendritic cell stimuli induce antitumour T-cell immunity. Nature 2015;521:99–104.
43. Germain C, Gnjatic S, Tamzalit F, Knockaert S, Remark R, Goc J, et al. Presence of B cells in tertiary lymphoid structures is associated with a protective immunity in patients with lung cancer. Am J Respir Crit Care Med 2014;189:832–44.
44. Yasuda M, Mizukami M, Hanagiri T, Shigematsu Y, Fukuyama T, Nagata Y, et al.Antigens recognized by IgG derived from tumor-infiltrating B lymphocytes in human lung cancer. Anticancer Res 2006;26:3607–11.
45. Kotlan B, Simsa P, Teillaud JL, Fridman WH, Toth J, McKnight M, et al. Novel ganglioside antigen identified by B cells in human medullary breast carcinomas: the proof of principle concerning the tumor-infiltrating B lymphocytes. J Immunol 2005;175:2278–85.
46. Hansen MH, Nielsen H, Ditzel HJ. The tumor-infiltrating B cell response in medullary breast cancer is oligoclonal and directed against the autoantigen actin exposed on the surface of apoptotic cancer cells. Proc Natl Acad Sci U S A 2001;98:12659–64.
47. Joyce JA, Fearon DT. T cell exclusion, immune privilege, and the tumor microenvironment. Science 2015;348:74–80.
48. Kanodia S, Da Silva DM, Karamanukyan T, Bogaert L, Fu YX, Kast WM. Expression of LIGHT/TNFSF14 combined with vaccination against human papillomavirus Type 16 E7 induces significant tumor regression. Cancer Res 2010;70:3955–64.
49. Maldonado L, Teague JE, Morrow MP, Jotova I, Wu TC, Wang C, et al. Intramuscular therapeutic vaccination targeting HPV16 induces T cell responses that localize in mucosal lesions. Sci Transl Med 2014;6: 221ra213.
50. Lutz ER, Wu AA, Bigelow E, Sharma R, Mo G, Soares K, et al.Immunotherapy converts nonimmunogenic pancreatic tumors into immunogenic foci of immune regulation. Cancer Immunol Res 2014;2:616–31.